Sensitivity study of experimental measures for the nuclear liquid-gas phase transition in the statistical multifragmentation model

W. Lin (林炜平),[1,2] P. Ren (任培培),[1,2] H. Zheng (郑华),[3,*] X. Liu (刘星泉),[2,†] M. Huang (黄美容),[4] R. Wada,[5] and G. Qu (曲国峰)[1,2]

[1]Key Laboratory of Radiation Physics and Technology of the Ministry of Education, Institute of Nuclear Science and Technology, Sichuan University, Chengdu 610064, China
[2]Institute of Modern Physics, Chinese Academy of Sciences, Lanzhou 730000, China
[3]Laboratori Nazionali del Sud, INFN, I-95123 Catania, Italy
[4]College of Physics and Electronics information, Inner Mongolia University for Nationalities, Tongliao 028000, China
[5]Cyclotron Institute, Texas A&M University, College Station, Texas 77843, USA

(Received 7 April 2018; published 23 May 2018)

The experimental measures of the multiplicity derivatives—the moment parameters, the bimodal parameter, the fluctuation of maximum fragment charge number (normalized variance of Z_{max}, or NVZ), the Fisher exponent (τ), and the Zipf law parameter (ξ)—are examined to search for the liquid-gas phase transition in nuclear multifragmention processes within the framework of the statistical multifragmentation model (SMM). The sensitivities of these measures are studied. All these measures predict a critical signature at or near to the critical point both for the primary and secondary fragments. Among these measures, the total multiplicity derivative and the NVZ provide accurate measures for the critical point from the final cold fragments as well as the primary fragments. The present study will provide a guide for future experiments and analyses in the study of the nuclear liquid-gas phase transition.

DOI: 10.1103/PhysRevC.97.054615

I. INTRODUCTION

The interest in multifragmentation processes, which were predicted a long time ago [1] and have been extensively studied following the advent of 4π detectors [2–4], lies in the fact that they provide a wealth of information on nuclear dynamics, on the properties of the nuclear equation of state (EOS), and on the possible nuclear liquid-gas phase transition. The nuclear liquid-gas phase transition in multifragmentation processes was first suggested in the early 1980s [5–7]. It is expected to occur when the nucleus is heated to a moderate temperature and breaks up on a short timescale into light particles and intermediate mass fragments with $Z \geqslant 3$ (IMF).

In the past three decades, many experimental and theoretical works have been devoted to searching for the liquid-gas phase transition in Fermi energy heavy-ion collisions and relativistic energy projectile fragmentations. Among the measures used for studies are the nuclear specific heat capacity (the caloric curves) [8–16], the bimodality in charge asymmetry [17–19], the Fisher droplet model analysis [20–26], the Landau free energy approach [25–31], the moment of the charge distributions [22,32–35], the fluctuation properties of the heaviest fragment size (charge) [22,23,35–37], Zipf's law [38,39], the multiplicity derivatives recently proposed by Mallik *et al.* [40], and the derivative of cluster size [41]. With these features, considerable progress has been accomplished on the theoretical as well as on the experimental side for the nuclear liquid-gas phase transition. Ma *et al.* in Refs. [22–24] examined most of these measures, except the multiplicity derivatives, as a function of the excitation energy, using rather light reaction systems of $^{40}Ar + ^{27}Al, ^{48}Ti$, and ^{58}Ni at 47 MeV/nucleon, and showed that all of them show a critical behavior around $E^*/A \sim 5.6$ MeV. However since all values of the measures are plotted as a function of the excitation energy, the signature appears as a broad peak around $E^*/A \sim 5.6$ MeV. Therefore, the specific properties of the nuclear liquid-gas phase transition in hot nuclear matter are still under debate and many efforts are still required.

In order to search for suitable observables in heavy-ion collisions, which can provide strong signatures for the nuclear liquid-gas phase transition and be a guide for future experiments, we investigate several experimental measures including the multiplicity derivatives, the moment parameters, and Zipf's law, and analyze the sensitivity of each observable in the framework of the statistical multifragmentation model (SMM) [42–47]. SMM is rather successful in describing the multiple production of intermediate mass fragments [48–50] and exhibits a phase transition of the liquid-gas type [51,52]. This article is organized as follows: A brief description of SMM is presented in Sec. II. The SMM calculations and analyses of phase transition are given in Sec. III. Discussions are given in Sec. IV. A brief summary is given in Sec. V.

II. STATISTICAL MULTIFRAGMENTATION MODEL (SMM)

In SMM, the fragmenting system is in thermal and chemical equilibrium at low density [44–47]. A Markov chain is

*zheng@lns.infn.it
†liuxingquan@impcas.ac.cn

generated to represent the whole partition ensemble in the version discussed below [45]. All breakup channels (partitions) for nucleons and excited fragments are considered under the conservation of mass, charge, momentum and energy. The primary fragments are described by liquid drops at a given freezeout volume. Light clusters with mass number $A \leqslant 4$ are considered as stable particles ("nuclear gas"). Their masses and spins are taken from the experimental values. Only translational degrees of freedom of these particles are taken into account in the entropy of the system. When the nuclear density becomes very low, the binding energy of clusters is significantly modified by the Pauli blocking and clusterization [53], but these effects are not taken into account in the SMM. Fragments with $A > 4$ are treated as spherical excited nuclear liquid drops and the free energies $F_{A,Z}$ are given as a sum of the bulk, surface, Coulomb, and symmetry-energy contributions:

$$F_{A,Z} = F^B_{A,Z} + F^S_{A,Z} + E^C_{A,Z} + F^{\rm sym}_{A,Z}, \tag{1}$$

where

$$F^B_{A,Z} = (-W_0 - T^2/\varepsilon_0)A, \tag{2}$$

$$F^S_{A,Z} = B_0 A^{2/3}\left[\frac{T_c^2 - T^2}{T_c^2 + T^2}\right]^{5/4}, \tag{3}$$

$$E^C_{A,Z} = \frac{3}{5}\frac{e^2}{r_0}[1 - (\rho/\rho_0)^{1/3}]\frac{Z^2}{A^{1/3}}, \tag{4}$$

$$F^{\rm sym}_{A,Z} = \gamma(A-2Z)^2/A - T S^{\rm sym}_{A,Z}. \tag{5}$$

$W_0 = 16$ MeV is used for the binding energy of infinite nuclear matter, and $\varepsilon_0 = 16$ MeV is related to the level density; $B_0 = 18$ MeV is used for the surface coefficient; $T_c = 18$ MeV is used for the critical temperature of infinite nuclear matter; e is the charge unit and $r_0 = 1.17$ fm; ρ is the density at the breakup and ρ_0 is the normal nuclear density; γ is the symmetry energy parameter; the $S^{\rm sym}_{A,Z}$ is the symmetry entropy of fragments, introduced in our previous work [47].

The entropy of fragments $S_{A,Z}$ can be derived from the free energy as

$$S_{A,Z} = -\frac{\partial F_{A,Z}}{\partial T} = S^B_{A,Z} + S^S_{A,Z} + S^{\rm sym}_{A,Z}. \tag{6}$$

After the primary breakup, the Coulomb acceleration and the secondary deexcitation are performed to get the final secondary fragments. In the deexcitation processes, the Fermi breakup of light primary fragments ($A < 16$), the successive particle emission ($A > 16$), and the fission of heavy nuclei ($A > 200$) are taken into account.

III. SMM CALCULATIONS AND ANALYSES OF PHASE TRANSITION

SMM calculations are performed with the source mass number $A_s = 100$, charge number $Z_s = 45$, and the fragmenting volume $V = 6V_0$, where V_0 is the volume at the normal nuclear density. The default symmetry energy coefficient $\gamma = 25$ MeV is used. The input source excitation energy (E_x) varies from 1 to 15 MeV/nucleon with an energy step of 0.25 MeV/nucleon. More than 1 million events are generated for each E_x. In order to be a guide in future experiments, the calculations are performed both for the primary and secondary fragments.

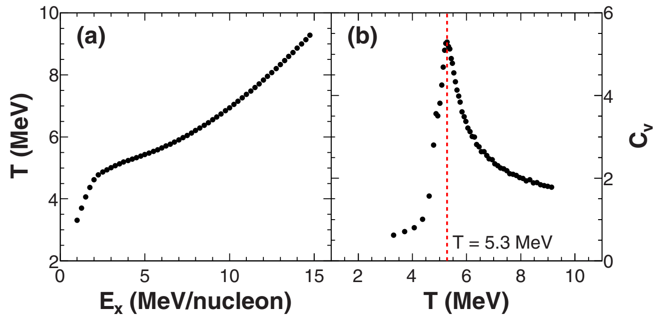

FIG. 1. (a) The caloric curve of a fragmenting source with $A_s = 100$, $Z_s = 45$ of SMM calculations. (b) The specific heat capacity C_v derived from the caloric curve as a function of source temperature. The vertical line shows the critical point at $T = 5.3$ MeV.

In SMM the "temperature" depends slightly on the fragmenting channel because of the energy fluctuates from partition to partition with the Markov-chain method. The energies are determined from the energy balance for a given partition. Therefore, the average value over all exit channels is used as the source temperature in the following analyses [47].

The specific heat capacity has long been considered to be a measure that should provide important information on the postulated nuclear liquid-gas phase transition [8,9,54–56]. As one can see from Fig. 1(a), a notable plateauing of the caloric curve is observed at $E_x \sim 4$ MeV for the SMM calculations, which results in a sharp increase of the specific heat capacity, C_v, as shown in Fig. 1(b). The sharp maximum of C_v strongly suggests that the liquid-gas phase transition occurs in SMM. The critical point at temperature $T = 5.3$ MeV is obtained. Experimentally the caloric curve has been measured in many experiments. The plateau of the caloric curve is qualitatively observed at an excitation energy of 5–10 MeV, depending on the system size [54]. However, due to the complexity of reaction mechanisms and sequential secondary decay processes, the experimental determination of the excitation energy and temperature becomes inaccurate and does not allow us to determine the critical point as a sharp transition, even if it is there. Therefore, it is crucial to find a good thermometer for the experiments, which will enable us to determine the temperature reliably and accurately and will have minimal effect from the sequential decay process. Here we will use $T = 5.3$ MeV as the theoretical critical point for the reference.

A. Multiplicity derivatives

The derivatives of total multiplicity and IMF multiplicity were recently proposed as an observable to search for nuclear liquid-gas phase transition by Mallik *et al.* in Ref. [40]. They showed that the multiplicity derivatives show a strong signature marking the first-order phase transition in the canonical thermodynamic model (CTM) [57], which is claimed to be essentially the same as SMM.

We apply the multiplicity derivatives to the fragmenting system calculated by SMM. Figures 2(a) and 2(b) show the

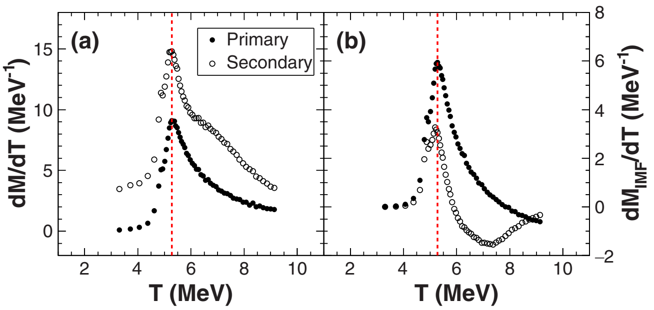

FIG. 2. (a) The total multiplicity derivatives of fragmenting system of SMM versus the source temperature. (b) Similar to (a) but for the derivatives of IMF multiplicity. The solid and open circles correspond to primary and secondary fragments, respectively. The vertical lines indicate the critical point at $T = 5.3$ MeV from Fig. 1(b).

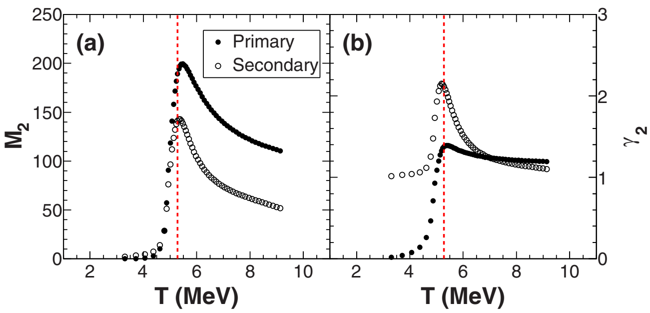

FIG. 3. (a) M_2 as a function of source temperature. (b) γ_2 as a function of source temperature. Solid and open circles correspond to primary and secondary fragments, respectively. The vertical lines indicate the critical point at $T = 5.3$ MeV from Fig. 1(b).

total and IMF multiplicity derivatives as a function of source temperature, respectively, for both primary (solid circles) and the secondary (open circles) fragments. All distributions show a sharp increase and have a maximum at or near the critical temperature of $T = 5.3$ MeV, shown by vertical lines in both figures. Good agreement between critical temperatures in the multiplicity derivatives and that in the specific heat capacity is found. The fact that only a slightly lower value ($\sim$0.1 MeV) is found in the IMF multiplicity derivative of secondary fragments indicates that the multiplicity derivatives provide a good measure in searching for the critical point of the nuclear matter liquid-gas phase transition. Our results are consistent with the conclusions in Ref. [40].

B. Moment parameters

The general definition of the kth moment [22,32,33] of charge distribution is given as

$$M_k = \sum_{Z_i \neq Z_{\max}} n_i Z_i^k, \tag{7}$$

where n_i is the multiplicity of fragments with charge number $Z = Z_i$ in each event. Using the zeroth (M_0), first (M_1), and second (M_2) moments, the quantity γ_2 is defined as

$$\gamma_2 = \frac{M_2 M_0}{M_1^2}. \tag{8}$$

M_2 and γ_2 are expected to show the critical point at which the fluctuations in fragment sizes become the largest [22,32,33]. Figure 3(a) and 3(b) show the results of M_2 and γ_2 as a function of source temperature, respectively. As one can see from Fig. 3(a), the M_2 of primary fragments shows a maximum at slightly higher ($\sim$0.2 MeV) temperature than the critical temperature $T = 5.3$ MeV, whereas the maximum of M_2 for secondary fragments is the same as the critical temperature. The maximum value of γ_2 of primary fragments appears at a temperature slightly larger than the critical temperature. In contrast, the maximum of γ_2 of secondary fragments is slightly lower than the critical temperature. The deviations of those in both the primary and secondary fragments are less than 0.1 MeV, as shown in Fig. 3(b).

C. Bimodal parameter and fluctuations of maximum fragments

The bimodality [17–19] is a double peaked distribution of an order parameter, which comes from the anomalous convexity of the underlying microcanonical entropy. It can be interpreted as the coexistence of different phases in the system and provides a definition of an order parameter as the best variable to separate the two maxima of the distribution [58]. In this framework, when a nuclear system is in the coexistence region, the probability distribution of the order parameter becomes bimodal. In Ref. [58], the sorting parameter with fragment atomic number $Z = 12$ as a limit between two phases, $(\sum_{Z_i \geqslant 13} Z_i - \sum_{3 \leqslant Z_i \leqslant 12} Z_i)/\sum_{Z_i \geqslant 3} Z_i$, which may connect with the density difference of the two phases ($\rho_L - \rho_G$), was chosen as the order parameter in the analysis of INDRA data.

As pointed out by Ma *et al.* in Ref. [22], the Z limit should be reduced between two phases for light systems, and the critical temperature appears at the inflection point of the bimodal parameter. In the present analysis, we choose $Z = 3$ as the limit between the two phases, and therefore the bimodal parameter can be defined as $(\sum_{Z_i \geqslant 4} Z_i - \sum_{1 \leqslant Z_i \leqslant 3} Z_i)/\sum_{Z_i \geqslant 1} Z_i$. Figure 4(a) shows the bimodal parameter as a function of source temperature. Lower temperatures of inflection point in bimodal parameter are found both for primary and secondary fragments compared to the critical temperature $T = 5.3$ MeV. This behavior is generally observed for the bimodal parameter when the sorting limit Z is changed to $4 < Z < 12$ and/or the light charged particles ($Z \leqslant 2$) from the sorting fragments are excluded.

The fluctuation of order parameter proposed by Botet in Ref. [59] provides a method to select an order parameter and characterize critical and off-critical behavior, without any equilibrium assumption. The fluctuations in the atomic number of the largest fragment ($Z_{\max}$) were applied in the analysis of INDRA data in Ref. [58], and the normalized variance of $Z_{\max}$ (NVZ) was utilized by Dorso *et al.* in Ref. [60] to investigate

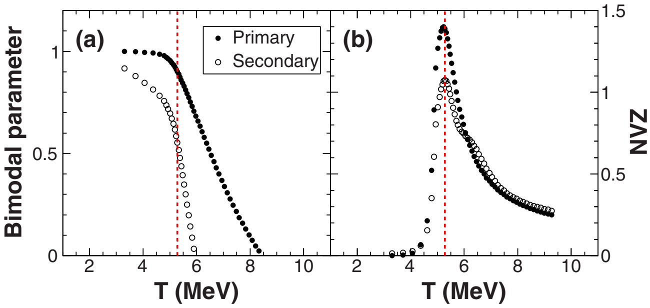

FIG. 4. (a) The bimodal parameter as a function of source temperature. (b) The NVZ as a function of source temperature. Solid and open circles correspond to that of primary and secondary fragments, respectively. The vertical lines indicate the critical point at $T = 5.3$ MeV from Fig. 1(b).

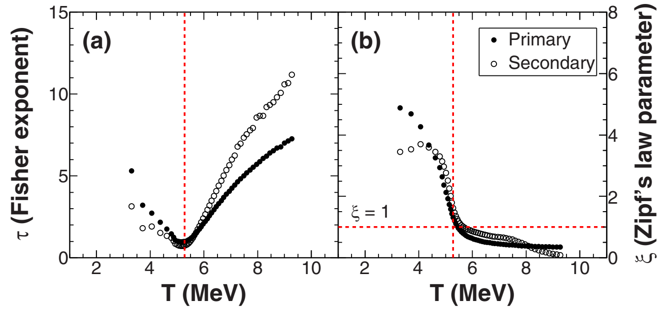

FIG. 5. (a) The Fisher exponent (τ) extracted from the Z distribution as a function of source temperature. (b) The Zipf law parameter (ξ) as a function of source temperature. Solid and open circles correspond to primary and secondary fragments, respectively. The vertical lines indicate the critical point at $T = 5.3$ MeV from Fig. 1(b). The horizontal line in (b) shows $\xi = 1$.

the fluctuation of $Z_{\max}$, which is given as

$$\mathrm{NVZ} = \frac{\sigma^2_{Z_{\max}}}{\langle Z_{\max}\rangle}. \tag{9}$$

In the SMM calculations, $Z_{\max}$ does not always show a Gaussian distribution. Therefore, we apply the root-mean-square (RMS) of $Z_{\max}$ as $\sigma_{Z_{\max}}$ in NVZ. Figure 4(b) shows the NVZ as a function of source temperature. One can see that the maxima of NVZ for both the primary and secondary fragments appear at the same temperature as that of the critical point, indicating that the NVZ also provides a good measure in searching for the critical point of the nuclear matter liquid-gas phase transition.

D. Fisher exponent and Zipf law parameter

The modified Fisher model (MFM) [20,25,61,62] has been extensively applied to the analysis of multifragmentation events since it was first adopted by Purdue's group in Refs. [6,7,63]. The fragment mass distributions in multifragmentation events are well described by a power-law distribution of $A^{-\tau}$ with the power-law exponent $\tau \sim 2.3$ [20,25,27].

In the framework of the MFM, the isotope yield in a multifragmentation reaction can be given as

$$Y(A,Z) = Y_0 A^{-\tau} \exp\left[-\frac{F(A,Z) - \mu_n N - \mu_p Z}{T}\right], \tag{10}$$

where $F(A,Z)$ is the free energy of a fragment with mass A and charge Z, and μ_n (μ_p) is the neutron (proton) chemical potential. At the critical point, the exponential term in Eq. (10) vanishes and the distribution becomes a pure power law,

$$Y(A) = Y_0 A^{-\tau}. \tag{11}$$

As shown by Ogul in Ref. [64], the power-law exponents of mass and charge distributions behave in a very similar fashion. Thus, we use $Z^{-\tau}$ to fit the charge distribution. To avoid contributions from fission-like large fragments ($Z > 20$) and from coalescence-like small clusters ($Z \leqslant 2$), we adopt the same range of $Z = 5$–15 in the fit as that in Ref. [65]. The extracted power-law exponents are shown in Fig. 5(a) both for the primary and secondary fragments. The minima of power-law exponents appear at slightly lower (~0.15 MeV) temperature both for the primary and secondary fragments compared to the critical temperature $T = 5.3$ MeV.

The fragments' hierarchy distribution gives another measure, proposed by Ma in Refs. [38,39], which provides a method to search for the liquid-gas phase transition in a finite system. It can be defined by the so-called Zipf plot, which is a plot of the relationship between mean sizes of fragments rank-ordered in size (i.e., the largest fragment, the second large fragment, the third large fragment, and so on). Originally the Zipf plot was used to analyze the hierarchy of usage of words in a language [66]. It has been applied in a broad variety of areas, such as population distributions, the size distribution of cities, the distribution in strengths of earthquakes, etc. The existence of very similar linear hierarchy distributions in these very different fields indicates that Zipf's law is a reflection of self-organized criticality [67].

We apply Zipf's law to the SMM events, in which the fragment charge number is employed as the variable to make a Zipf-type plot, and the resultant distributions are fitted with a power law,

$$\langle Z_{\mathrm{rank}}\rangle \propto \mathrm{rank}^{-\xi}, \tag{12}$$

where rank $= i$ for the ith largest fragment. ξ is the Zipf law parameter. When $\xi \sim 1$, Zipf's law is satisfied. The extracted ξ values are plotted as a function of source temperature in Fig. 5(b) both for the primary and secondary fragments. One can see from the figure that Zipf's law is satisfied at a temperature slightly larger than the critical temperature both for the primary and secondary fragments.

IV. DISCUSSIONS

In Sec. III, we investigated several experimental measures that provide signatures for the nuclear liquid-gas phase transition in heavy-ion collisions in the framework of SMM both for the primary and secondary fragments. All these measures predict a critical temperature at or near to that from the specific heat capacity when they are plotted as a function of the source temperature. From the experimental point of view, it is important to provide measures which show the same signature

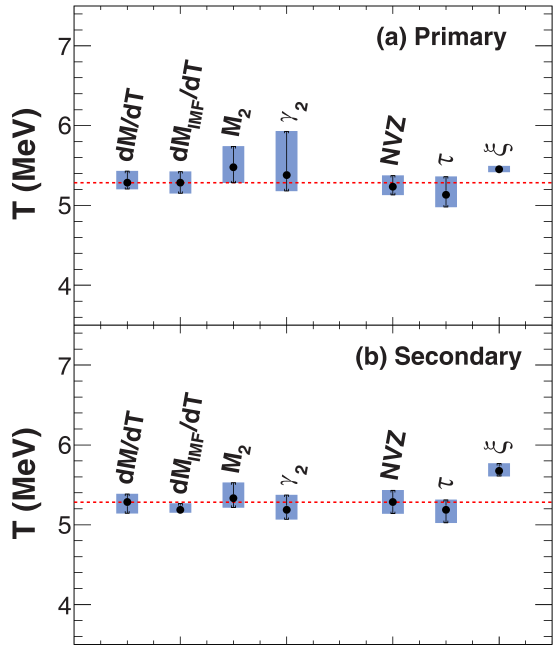

FIG. 6. (a) The sensitivities in the critical temperature of primary fragments for all the measures except for bimodal parameter. (b) The same as (a) but for secondary fragments. The horizontal lines indicate the critical point at $T = 5.3$ MeV from Fig. 1(b). Solid circles correspond to the critical temperature extracted by each measure. For the error bars shown by the shaded area, see the detail in the text.

for the primary and secondary particles in the study of the nuclear liquid-gas phase transition.

Due to the experimental errors (statistical and systematic), there will be some uncertainties included in the measures. Therefore, the sensitivities of these measures were further studied. The uncertainty, ΔT, is evaluated as a quantitative measure when 5% deviation from the maximum or minimum value is observed at $T = T_c \pm \Delta T$. Figure 6 shows the sensitivities of all these measures except for the bimodal parameter, in which the inflection point is used to obtain the critical point and does not show the minimum or maximum value. One can easily get from the figure that the total multiplicity derivative and NVZ have the same critical temperature as that of the specific heat capacity both for the primary and secondary fragments. Moreover, the small errors in temperature in Figs. 6(a) and 6(b) indicate that the total multiplicity derivative and NVZ are the best measures in the study of the nuclear liquid-gas phase transition.

All the other measures are noticeably affected by the secondary decay, as one can see in Figs. 6(a) and 6(b). The critical temperatures (solid circles) extracted from primary and secondary fragments are slightly different. The IMF multiplicity derivative is found at exactly the critical temperature for the primary fragments. But due to the secondary decay effect, the extracted critical point appears at slightly lower temperature for the secondary fragments. In contrast, the measures of M_2 and the Fisher exponent τ predict an accurate critical temperature for the secondary fragments, but show slightly higher temperature for M_2 and lower temperature for τ for the primary fragments. The γ_2 is found to have similar accuracy in both the primary and secondary fragments, though a large error bar is obtained for primary fragments. In addition, the temperature error bars are also smaller for M_2, γ_2, and τ for the secondary fragments, which indicates that these measures are more sensitive for the secondary fragments. The Zipf law parameter ξ shows a critical temperature slightly larger than that from the specific heat capacity for primary fragments. But due to its sharp response, the temperature error bar still does not cover the critical temperature from specific heat capacity. The result from secondary fragments is much worse for the Zipf law parameter (ξ).

From the above comparisons, we conclude that the total multiplicity derivative and NVZ are the best measures with which to predict the critical point accurately, with a minimal uncertainty both for the primary and secondary fragments.

V. SUMMARY

The multiplicity derivatives, the moment parameters, the bimodal parameter, the fluctuation of maximum fragment charge number (NVZ), the Fisher exponent (τ), and the Zipf law parameter (ξ) are examined as the measures to search for the liquid-gas phase transition in nuclear multifragmention processes within the framework of SMM. The sensitivities of these measures are studied. All these measures predict a critical signature at or near to the critical point extracted from the specific heat. Among these measures, the total multiplicity derivative and NVZ are found to be the best measures in accuracy and sensitivity for the first-order phase transition even after the secondary decay process. The IMF multiplicity derivative is found to be accurate in the primary fragments but shows a slight deviation from the critical temperature in the secondary fragments. In contrast, the M_2 and the Fisher exponent τ observables predict the critical point very well from the secondary fragments, but show a slight deviation for the primary fragments. The γ_2 shows similar accuracy (less than 0.1 MeV deviation) both for the primary and secondary fragments. The smaller temperature error bars for the secondary fragments indicate the measures of M_2, γ_2, and τ are more sensitive for the secondary fragments. A lower temperature is predicted by the bimodal parameter both for the primary and secondary fragments, while the Zipf law parameter ξ predicts higher temperatures both for the primary and secondary fragments. These investigations should provide a guide for future experiments and analyses in the study of the nuclear liquid-gas phase transition.

ACKNOWLEDGMENTS

The authors thank A. S. Botvina for providing his code. This work is supported by the National Key Research and Development program (MOST 2016YFA0400501), the National Natural Science Foundation of China (Grant No. 11705242), the Program for the CAS "Light of West China" (No. 29Y601030), and the Fundamental Research Funds For the Central Universities (No. YJ201820). This work is also supported by the U.S. Department of Energy under Grant No. DE–FG02–93ER40773.

[1] N. Bohr, Nature (London) **137**, 344 (1936).
[2] B. Borderie and M. F. Rivet, Prog. Part. Nucl. Phys. **61**, 551 (2008).
[3] F. Gulminelli, W. Trautmann, S. J. Yennello, and Ph. Chomaz, Eur. Phys. J. A **30**, 1 (2006), and related topics in the issue.
[4] Ph. Chomaz, M. Colonna, and J. Randrup, Phys. Rep. **389**, 263 (2004).
[5] J. E. Finn, S. Agarwal, A. Bujak *et al.*, Phys. Rev. Lett. **49**, 1321 (1982).
[6] R. W. Minich, S. Agarwal, A. Bujak *et al.*, Phys. Lett. B **118**, 458 (1982).
[7] A. S. Hirsch, A. Bujak, E. Finn *et al.*, Nucl. Phys. A **418**, 267 (1984).
[8] E. Suraud, C. Grégoire, and B. Tamain, Prog. Part. Nucl. Phys. **23**, 357 (1989), and references therein.
[9] D. H. E. Gross, Prog. Part. Nucl. Phys. **30**, 155 (1993), and references therein.
[10] K. Hagel, D. Fabris, P. Gonthier *et al.*, Nucl. Phys. A **486**, 429 (1988).
[11] R. Wada, D. Fabris, K. Hagel *et al.*, Phys. Rev. C **39**, 497 (1989).
[12] D. Cussol, G. Bizard, R. Brou *et al.*, Nucl. Phys. A **561**, 298 (1993).
[13] J. Pochodzalla, T. Möhlenkamp, T. Rubehn *et al.*, Phys. Rev. Lett. **75**, 1040 (1995).
[14] R. Wada, R. Tezkratt, K. Hagel *et al.*, Phys. Rev. C **55**, 227 (1997).
[15] K. Hagel, R. Wada, J. Cibor *et al.*, Phys. Rev. C **62**, 034607 (2000).
[16] T. Furuta and A. Ono, Phys. Rev. C **74**, 014612 (2006).
[17] O. Lopez, D. Lacroix, and E. Vient, Phys. Rev. Lett. **95**, 242701 (2005).
[18] M. Pichon, B. Tamain, R. Bougault *et al.* (INDRA and ALADIN Collaborations), Nucl. Phys. A **779**, 267 (2006).
[19] B. Borderie, E. Bonnet, F. Gulminelli *et al.* (INDRA and ALADIN Collaborations), Nucl. Phys. A **834**, 535c (2010).
[20] M. E. Fisher, Rep. Prog. Phys. **30**, 615 (1969); Physics Physique Fizika **3**, 255 (1967).
[21] J. B. Elliott, L. G. Moretto, L. Phair *et al.*, Phys. Rev. Lett. **88**, 042701 (2002).
[22] Y. G. Ma, J. B. Natowitz, R. Wada *et al.*, Phys. Rev. C **71**, 054606 (2005).
[23] Y. G. Ma, J. B. Natowitz, R. Wada *et al.*, Nucl. Phys. A **749**, 106 (2005).
[24] Y. G. Ma, R. Wada, K. Hagel *et al.*, Phys. Rev. C **69**, 031604(R) (2004).
[25] M. Huang, R. Wada, Z. Chen *et al.*, Phys. Rev. C **82**, 054602 (2010).
[26] G. Giuliani, H. Zheng, and A. Bonasera, Prog. Part. Nucl. Phys. **76**, 116 (2014).
[27] A. Bonasera, Z. Chen, R. Wada *et al.*, Phys. Rev. Lett. **101**, 122702 (2008).
[28] R. Tripathi, A. Bonasera, S. Wuenschel *et al.*, Phys. Rev. C **83**, 054609 (2011).
[29] R. Tripathi, A. Bonasera, S. Wuenschel *et al.*, J. Phys. Conf. Ser. **312**, 082043 (2011).
[30] R. Tripathi, A. Bonasera, S. Wuenschel *et al.*, Int. J. Mod. Phys. E **21**, 1250019 (2012).
[31] J. Mabiala, A. Bonasera, H. Zheng *et al.*, Phys. Rev. C **87**, 017603 (2013).
[32] X. Campi, Phys. Lett. B **208**, 351 (1988).
[33] X. Campi, J. Phys. A **19**, L917 (1986).
[34] S. Das Gupta and A. Z. Mekjian, Phys. Rev. C **57**, 1361 (1998).
[35] P. F. Mastinu, M. Belkacem, F. Gramegna, and P. M. Milazzo, Phys. Rev. C **57**, 831 (1998).
[36] R. Botet, M. Ploszajczak, A. Chbihi, B. Borderie, D. Durand, and J. Frankland, Phys. Rev. Lett. **86**, 3514 (2001).
[37] J. D. Frankland, A. Chbihi, A. Mignon *et al.* (INDRA and ALADIN Collaborations), Phys. Rev. C **71**, 034607 (2005).
[38] Y. G. Ma, Phys. Rev. Lett. **83**, 3617 (1999).
[39] Y. G. Ma, Eur. Phys. J. A **6**, 367 (1999).
[40] S. Mallik, G. Chaudhuri, P. Das, and S. Das Gupta, Phys. Rev. C **95**, 061601(R) (2017).
[41] P. Das, S. Mallik, and G. Chaudhuri, arXiv:1802.07020.
[42] X. Z. Zhang, D. H. E. Gross, S. Y. Xu, and Y. M. Zheng, Nucl. Phys. A **461**, 641 (1987).
[43] X. Z. Zhang, D. H. E. Gross, S. Y. Xu, and Y. M. Zheng, Nucl. Phys. A **461**, 668 (1987).
[44] J. P. Bondorf, A. S. Botvina, A. S. Iljinov, I. N. Mishustin, and K. Sneppen, Phys. Rep. **257**, 133 (1995).
[45] A. S. Botvina and I. N. Mishustin, Phys. Rev. C **63**, 061601(R) (2001).
[46] G. A. Souliotis, A. S. Botvina, D. V. Shetty, A. L. Keksis, M. Jandel, M. Veselsky, and S. J. Yennello, Phys. Rev. C **75**, 011601(R) (2007).
[47] W. Lin, H. Zheng, P. Ren *et al.*, Phys. Rev. C **97**, 044603 (2018).
[48] A. S. Botvina, I. N. Mishustin, M. Begemann-Blaich *et al.*, Nucl. Phys. A **584**, 737 (1995).
[49] M. D'Agostino, A. S. Botvina, P. M. Milazzo *et al.*, Phys. Lett. B **371**, 175 (1996).
[50] M. D'Agostino, A. S. Botvina, M. Bruno *et al.*, Nucl. Phys. A **650**, 329 (1999).
[51] N. Buyukcizmeci, R. Ogul, and A. S. Botvina, Eur. Phys. J. A **25**, 57 (2005).
[52] R. Ogul, N. Buyukcizmeci, and A. S. Botvina, Nucl. Phys. A **749**, 126c (2005).
[53] S. Typel, G. Röpke, T. Klähn, D. Blaschke, and H. H. Wolter, Phys. Rev. C **81**, 015803 (2010).
[54] J. B. Natowitz, R. Wada, K. Hagel *et al.*, Phys. Rev. C **65**, 034618 (2002)
[55] M. D'Agostino, F. Gulminelli, Ph. Chomaz *et al.*, Phys. Lett. B **473**, 219 (2000).
[56] M. D'Agostino, R. Bougault, F. Gulminelli *et al.*, Nucl. Phys. A **699**, 795 (2002).
[57] C. B. Das, S. Das Gupta, W. G. Lynch, A. Z. Mekjian, and M. B. Tsang, Phys. Rep. **406**, 1 (2005).
[58] B. Borderie, J. Phys. G **28**, 217(R) (2002).
[59] R. Botet and M. Płoszajczak, Phys. Rev. E **62**, 1825 (2000).
[60] C. O. Dorso, V. C. Latora, and A. Bonasera, Phys. Rev. C **60**, 034606 (1999).
[61] A. Bonasera, M. Bruno, C. O. Dorso, and P. F. Mastinu, Rivista Del Nuovo Cimento **23**, 1 (2000).
[62] W. Lin, X. Liu, M. R. D. Rodrigues *et al.*, Phys. Rev. C **89**, 021601(R) (2014); **95**, 039907(E) (2017).
[63] A. S. Hirsch, A. Bujak, J. E. Finn *et al.*, Phys. Rev. C **29**, 508 (1984).

[64] R. Ogul and A. S. Botvina, Phys. Rev. C **66**, 051601(R) (2002).

[65] A. S. Botvina, N. Buyukcizmeci, M. Erdogan, J. Lukasik, I. N. Mishustin, R. Ogul, and W. Trautmann, Phys. Rev. C **74**, 044609 (2006).

[66] G. K. Zipf, *Human Behavior and the Principle of Least Effort* (Addisson-Wesley, Cambridge, MA, 1949); D. Crystal, *The Cambridge Encyclopedia of Language* (Cambridge University, Cambridge, UK, 1987), p. 86.

[67] D. L. Turcotte, Rep. Prog. Phys. **62**, 1377 (1999).